Probing gas disc physics with LISA: simulations of an intermediate mass ratio inspiral in an accretion disc

A. M. Derdzinski^{1*}, D. D'Orazio², P. Duffell², Z. Haiman¹, A. MacFadyen³

¹Department of Astronomy, Columbia University, New York, NY, 10027, USA

Received / Accepted

ABSTRACT

The coalescence of a compact object with a $10^4 - 10^7 M_{\odot}$ supermassive black hole (SMBH) produces mHz gravitational waves (GWs) detectable by the future Laser Interferometer Space Antenna (LISA). If such an inspiral occurs in the accretion disc of an active galactic nucleus (AGN), the gas torques imprint a small deviation in the GW waveform. Here we present two-dimensional hydrodynamical simulations with the moving-mesh code DISCO of a BH inspiraling at the GW rate in a binary system with a mass ratio $q = M_2/M_1 = 10^{-3}$, embedded in an accretion disc. We assume a locally isothermal equation of state for the gas (with Mach number $\mathcal{M}=20$) and implement a standard α -prescription for its viscosity (with $\alpha=0.03$). We find disc torques on the binary that are weaker than in previous semi-analytic toy models, and are in the opposite direction: the gas disc slows down, rather than speeds up the inspiral. We compute the resulting deviations in the GW waveform, which scale linearly with the mass of the disc. The SNR of these deviations accumulates mostly at high frequencies, and becomes detectable in a 5-year LISA observation if the total phase shift exceeds a few radians. We find that this occurs if the disc surface density exceeds $\Sigma_0 \gtrsim 10^{2-3} {\rm g \, cm^{-2}}$, as may be the case in thin discs with near-Eddington accretion rates. Since the characteristic imprint on the GW signal is strongly dependent on disc parameters, a LISA detection of an intermediate mass ratio inspiral would probe the physics of AGN discs and migration.

Key words: black hole physics, gravitational waves, hydrodynamics

1 INTRODUCTION

LISA is currently planned to launch by 2034 and is expected to herald the era of space-based interferometry with the detection of gravitational waves (GWs) at wavelengths larger than the Earth. With an interferometer arm-length of 2.5 million km, LISA will probe the mHz GW sky with the primary goal of detecting merging supermassive black holes (SMBHs) throughout cosmic history. While the loudest sources in the LISA frequency band include merging SMBHs with component masses $M_{\rm BH} \sim 10^4 - 10^7 M_{\odot}$ up to a redshift $z \sim 20$, LISA will also be sensitive to less massive compact objects coalescing with SMBHs. These events are referred to as intermediate mass ratio inspirals (IMRIs; $q \equiv M_2/M_1 \approx 10^{-3} - 10^{-4}$) or extreme mass ratio inspirals (EMRIs; $q \lesssim 10^{-4}$, detectable up to $z \sim 4$, Amaro-Seoane et al. 2017).

Unlike stellar-mass BH mergers which are presumed to occur in vacuum (although see Perna et al. 2016; Janiuk et al. 2017; Bartos et al. 2017; McKernan et al. 2017; Stone et al. 2017; D'Orazio & Loeb 2018), many LISA events may occur in gaseous environments in galactic nuclei. Only $\sim 1\%$ of galaxies host active galactic nuclei

* E-mail: aderdzinski@astro.columbia.edu

(AGN), in which the central SMBH is accreting at nearly the Eddington rate from a thin, cold accretion disc, but there is plenty of evidence that AGN are triggered by galactic mergers (e.g. Kauffmann & Haehnelt 2000; Hopkins et al. 2008; Goulding et al. 2018 and references therein). In particular, the merger of two massive galaxies results in a supply of gas that flows into the nucleus of the post-merger remnant (Dotti et al. 2012; Barnes & Hernquist 1996), providing a gas-rich environment for BH accretion. As a result, a large fraction of SMBH mergers are expected to occur in a gaseous environment (see, e.g. Mayer 2013 for a review).

If a coalescing compact BH binary encounters a sufficient amount of gas, it will experience a gravitational torque that can act to either accelerate or hinder a GW-driven inspiral. The presence of gas also provides the opportunity for BHs to accrete, which in turn will affect their mass, spin, and momentum. This raises an important question: could gas change the orbital evolution of a binary sufficiently strongly such that the corresponding changes in the GW waveform become measurable? If it does, the GW signal would not only provide information about the source parameters, but it also would carry a characteristic signature of the environment in which the source originated.

Thus far the impact of gaseous forces on GW signals has

²Department of Astronomy, Harvard University, 60 Garden Street Cambridge, MA 01238, USA

³Center for Cosmology and Particle Physics, Physics Department, New York University, New York, NY 10003, USA

been addressed only via semi-analytical toy models (Kocsis et al. 2011; Yunes et al. 2011; Barausse et al. 2014, 2015b). The overall conclusion from these studies is that gas has a negligible impact for SMBH binaries in the LISA band, except for systems with extreme mass ratios ($q \ll 1$). Environmental influences become important for sources with less massive companions, where GWs are weaker and gas effects are comparatively stronger. Semi-analytical estimates by Kocsis et al. 2011 focused on EMRIs and found that a dense, near-Eddington gas disc can speed up the inspiral to an extent observable by LISA.

GW sources with $q \ll 1$ include a range of possible SMBH component masses, but in the present study we focus on IMRIs that will fall in the mHz GW band. The two relevant cases in this regime include the mergers of massive stellar remnant BHs ($M_{\rm BH}$ ~ $10-100M_{\odot}$) with IMBHs ($M_{\rm BH} \sim 10^{4-5} M_{\odot}$), or $10^{3-4} M_{\odot}$ IMBHs coalescing into $10^{6-7} M_{\odot}$ SMBHs. For our detectability estimates we adopt the specific case of a $q = 10^{-3}$ mass-ratio binary with a primary BH mass of $M_1 = 10^6 M_{\odot}$.

IMRI rate estimates predict a few to tens of mergers per year in the universe (Amaro-Seoane et al. 2007; Miller 2009). These estimates are based on stellar dynamical processes in galactic nuclei, and only a small fraction of these events would be expected to occur in a gaseous environment. However, IMRIs could also occur in AGN discs via several additional evolutionary pathways, either from compact objects in the galactic nucleus whose orbits are dragged into the plane of the disc by repeatedly crossing the disc (e.g. Ivanov et al. 1999; McKernan et al. 2012; Kennedy et al. 2016 and references therein), or from compact remnants that are formed in the disc in the first place (e.g. Goodman & Tan 2004; Levin 2007; McKernan et al. 2014; see also Stone et al. 2017). Subsequent accretion and mergers of these remnants can lead to IMBHS embedded in AGN discs (e.g. Bellovary et al. 2016; Yi et al. 2018). Similarly to near equal-mass SMBH mergers, E/IMRIs may preferentially occur in AGN discs.

The previous studies mentioned above estimate the gas impact on E/IMRIs in near-Eddington accretion discs with semi-analytical models of the so-called migration torque. For IMRIs in particular, these migration torques are based on the viscous torque and are estimated for a non-inspiraling perturber on a fixed circular orbit. However, a rapidly inspiraling, GW-driven perturber modifies the disc structure differently from a non-migrating perturber. As a result, the torques for a moving perturber differ in both strength and sign from the torques for a perturber on a fixed orbit (Duffell et al. 2014), and should also evolve differently during the inspiral.

Motivated by the above, in this paper we perform highresolution two-dimensional (2D) hydrodynamical simulations, and we directly measure the torques exerted on an IMBH embedded in the accretion disc of a central SMBH. We use the moving-mesh grid code DISCO (Duffell 2016), model the IMBH as a sink particle, and assume its orbit follows a GW-driven inspiral. The disc is assumed to have a locally isothermal equation of state and to obey a standard α -prescription for its viscosity. We calculate the impact of the disc torques throughout the coalescence, and predict the corresponding modification to the GW waveform seen by LISA. We also compute the signal-to-noise ratio (SNR) of the detectability of these modifications.

Focusing on the intermediate mass-ratio regime has two advantages compared to EMRIs. First, the inspiral is more rapid, allowing us to simulate a large portion of the inspiral as it traces out a broad range of orbital separations and frequencies. Second, the system is easier to resolve numerically, allowing us to follow the system for as many as $\approx 10,000$ binary orbits.

Our primary goal is to estimate the detectability of the gas imprint on an IMRI with the currently proposed LISA configuration (Klein et al. 2016). The torques scale linearly with the mass of the AGN disc involved, and also depend on other disc properties, such as temperature and viscosity. Therefore, a measurement of a gas imprint on the inspiral waveform should probe the properties of the accretion disc in which the source resides.

This paper is organised as follows. In § 2, we summarise previous work on migration torques in more detail. In § 3, we describe our simulation setup, and in § 4 we present our results, focusing on the torque measurements. In § 5 we use the measured torques to compute the modifications of the GW signal and estimate their detectability with LISA. In § 6, we discuss our results, along with some caveats, and finally in § 7 we summarise our conclusions and the implications of this work.

2 PREVIOUS WORK ON MIGRATION TORQUES FOR **GW SOURCES**

Early estimates of the impact of a gas disc on the gravitational waveforms of a compact object (CO) spiraling into a SMBH appear in Chakrabarti (1996) and Narayan (2000). These studies focused on the angular momentum exchange between the CO and the disc due to accretion and hydrodynamical drag in disc models at different radiative efficiencies. Levin (2007) considered, additionally, the impact of torques from density waves excited in a thin accretion disc (Goldreich & Tremaine 1980), often called "Type I torques" in the context of extrasolar planets (see below). The impact of a broader range of environmental effects on EMRI gravitational waveforms has been enumerated in Yunes et al. (2011) and Barausse et al. (2015a).

These studies found that the effect of gas is generally very weak and undetectable for LISA sources. The exceptions are systems with a small ratio, for which the gas torques due to the tidal deformation of the disc (so-called migration torques) can produce detectable deviations to the GW torque. Such disc torques are more extensively studied in the context of protoplanetary discs and planet migration, including numerous two- and three-dimensional hydrodynamical simulations (see a review by, e.g. Baruteau et al. 2014).

In the protoplanetary disc context, migration is described by two limiting cases (Type I and Type II; Ward 1997). Type I torques on low mass-ratio planet systems ($q < 10^{-4}$) are well understood, in the sense that they can be described by a linear perturbation theory (Goldreich & Tremaine 1980), which is successfully reproduced in numerical studies (e.g. Tanaka et al. 2002). However, these torques can be sensitive to disc thermodynamics (Paardekooper & Mellema 2006). Type II migration concerns more massive planets that can carve gaps in their discs (for intermediate masses $q > 10^{-3}$, with the precise value depending on the disc viscosity and temperature). In this regime the torques become nonlinear, so there is no analytical solution for the migration rate. Often, semi-analytical estimates are based on the viscous torque, but hydrodynamical simulations show that migration in this regime can deviate significantly from the viscous rate (Edgar 2007; Crida & Morbidelli 2007; Duffell et al. 2014; Robert et al. 2018). For intermediate mass perturbers

¹ It is worth noting that gas discs could be much more important, and produce order-unity effects, for the more massive, sub-parsec separation ~ 109 M_☉ SMBH binaries at nano-Hz frequencies, detectable by pulsar timing arrays (Kocsis & Sesana 2011; Tanaka et al. 2012; Sesana et al. 2012).

in particular, the torque develops a nonlinear component that is remarkably sensitive to disc parameters such as the viscosity, Mach number, and density gradient (Duffell 2015a).

In the context of binaries embedded in AGN discs, Yunes et al. (2011) and Kocsis et al. (2011) computed modified waveforms, using semi-analytical formulae of the above planetary migration torques, for both extreme and intermediate-mass perturbers. Kocsis et al. (2011), in particular, showed that the gas-induced drift in the accumulated GW phase can exceed a few radians per year (depending on disc parameters), a limit that is detectable with LISA's sensitivity. For the most massive disc models, the drift can become as large as 1,000 radians per year, which provides the possibility for LISA to accurately probe disc parameters (possibly limited by degeneracies between migration and system parameters).

In our present study, we focus on the analog of gap-opening satellites (for $q=10^{-3}$) in the context of BHs. While similar to the planet case, there are three major differences: (1) the BHs accrete, which is typically ignored when calculating planetary torques, (2) the BH orbit is strongly dominated by GWs (in the LISA band), there is no analogous "external" force in the planet case, and (3) the physical parameters of AGN discs differ from protoplanetary discs, which are typically thicker (lower Mach number) and have a lower viscosity.

The combination of these effects on migration torques has not been studied in detail in any simulation to date. For completeness, we note that related works exist, which present simulations of gas discs that include unequal-mass, GW-driven binaries, both in 1D (Chang et al. 2010; Fontecilla et al. 2017; Tazzari & Lodato 2015) and in 3D (Baruteau et al. 2012; Cerioli et al. 2016). These studies aimed at understanding the tidal squeezing of the inner disc by the inspiraling companion (a 'snow-plow' effect), and the resulting enhanced accretion rate onto the primary BH and electromagnetic (EM) emission. These works did not measure the gas torques on the binary. Likewise, recent 2D simulations followed the GW-driven inspiral of an equal-mass SMBH binary (Farris et al. 2015b; Tang et al. 2018) in the LISA band, but focused on the accretion rates and electromagnetic (EM) emission, and did not measure the torques in this regime.

Finally, we note the work of Duffell et al. (2014), whose results directly inspired the present study. These authors measured the torques on a Jupiter-like planet $(q = 10^{-3})$, embedded in a protoplanetary disc, and migrating at a broad range of manually prescribed rates. By measuring the torques as a function of the rate at which the planet is dragged inward, a unique migration rate can be identified that is consistent with the torques measured at that rate. This is meant as a "trick" to avoid a numerically challenging simulation of a "live" binary coupled to the disc. However, as a by-product, Duffell et al. (2014) inadvertently studied migration in a case similar to GW-driven inspiral. They found that above some migration rate $(a(da/dt)^{-1} \gtrsim 10^5 t_{\rm orb} \sim t_{\rm visc}$, where a is the binary separation, $t_{\rm orb}$ is its orbital period, and $t_{\rm visc}$ the viscous timescale), the gas torques are modified. Interestingly, at sufficiently rapid migration rates, the torques change sign and start to slow down, rather than speed up, the inspiral. While their study focused on non-accreting planets in protoplanetary discs, the dependence of torques on migration rate implies that the gas torques of a non-migrating secondary cannot simply be linearly added to the much larger external torques (in our case, from GWs).

In summary, in the present paper, we extend semi-analytic estimates of the modified GW waveforms (Kocsis et al. 2011), by running hydrodynamic simulations with a setup similar to Duffell et al. (2014), except with the addition of accretion, GW-driven

migration, and a more AGN-like disc model. We expect that the torques we measure will be very sensitive to disc parameters, and therefore this study is but the first step toward a complete exploration of the importance of gas discs for LISA sources (Derdzinski et al, in prep).

3 NUMERICAL METHODS

3.1 Disc Model

Our model is a two-dimensional, locally isothermal, viscous gas disc, evolved using the moving-mesh grid code DISCO (Duffell 2016). DISCO is idealised for modeling accretion discs as it has the capability to allow the grid to move with the Keplerian flow of the gas, thus reducing advection errors produced by shearing flow between grid cells.

The computation domain extends from $0.5 \le r/r_0 \le 2.75$ where r is measured from the primary BH which is held at the origin, and r_0 is an arbitrary distance unit set to $r_0 = 1$. Likewise, the primary mass is set to $GM_1 = 1$ in code units (where G is the gravitational constant). Note that the orbital time in code units at $r = r_0$ (the final binary separation) is 2π . The grid is logarithmically spaced in polar coordinates, with a total of 512 radial cells and an increasing number of azimuthal cells at outer radii such that the aspect ratio of each cell is unity. This resolution reaches 30 zones per scale height, which is important for capturing the gas morphology around the secondary BH. To ensure that our resolution is adequate, we have performed a test run with 800 radial grid cells, and found that our measured torques do not change. We employ Dirichlet (fixed) conditions at the inner and outer boundaries to ensure a constant mass flux rate.

The disc is parameterised by a constant aspect ratio $h/r = \mathcal{M}^{-1}$, where h is the disc scale height, r is the distance from the SMBH, and \mathcal{M} is the Mach number, assumed to be independent of r. Under this assumption, gas dynamics is scale-free as the black hole migrates through the domain, and the sound speed varies as $c_S = v_{\phi}/\mathcal{M}$, where $v_{\phi} = r\Omega$ is the orbital velocity and Ω is the initial Keplerian orbital frequency at r. We assume the disc is gas pressure dominated, neglecting radiation pressure. Viscosity is set with an α -law prescription, with the kinematic viscosity provided by $v = \alpha c_S h$. We neglect radiative cooling and instead assume the disc is locally isothermal (the temperature profile and corresponding mach number remains fixed) by setting the vertically integrated pressure to $p = c_S^2 \Sigma(r)$. Here $\Sigma(r)$ is the vertically-integrated surface density, which is assumed to follow

$$\Sigma(r) = \Sigma_0 \left(\frac{r}{r_0}\right)^{-1/2},\tag{1}$$

where $\Sigma_0 \equiv \Sigma(r_0)$ is a constant scaling factor. Since the orbit of the secondary BH is imposed by hand (§ 3.2) and we have no self-gravity, Σ_0 can be scaled to any value. Gas forces on the BH simply scale linearly with Σ_0 , as long as Σ_0 remains low enough not to significantly modify the orbit. This assumes that the evolution of the binary is overwhelmingly dominated by GWs, which we show to be valid in § 4.1 below.

For parameters describing the disc temperature and viscosity, we choose $\mathcal{M}=20$ and $\alpha=0.03$. While neither of these values are typical of what we expect in AGN discs (where we believe the gas is highly supersonic, with $\mathcal{M}\sim 100$ and highly ionised leading to $\alpha\sim 0.1-0.3$), we implement these values here because they are (i) numerically easier to simulate and (ii) this particular combination of

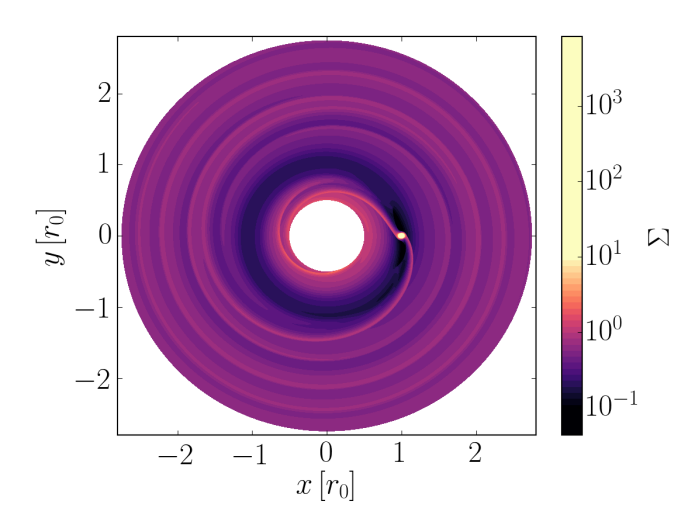


Figure 1. The logarithmic surface density over the whole computational domain, at the end of a simulation run. The primary BH is at the origin, and the gas disc and the secondary BH are both orbiting counter-clockwise. The secondary BH is located at (x, y) = (1, 0), marked by a large overdensity.

 ${\cal M}$ and α leads to a gap with a similar depth to a disc with AGN-like parameters.

Fig. 1 shows a snapshot of the logarithmic 2D surface density over the whole computational domain, at the end of an illustrative run.

3.2 The migrator and the GW inspiral

The primary BH is held at the origin which is excised from the simulation domain. The secondary BH is placed in a prograde orbit, and modeled by a 'vertically averaged' potential of the form

$$\Phi_2 = \frac{GM_2}{(r_2^2 + \epsilon^2)^{1/2}},\tag{2}$$

where r_2 is the distance to the secondary BH and ϵ is a smoothing length, which we set to one half the scale height. **This approach essentially neglects the gravitational pull of the secondary from within** $r_2 < \epsilon < r/\mathcal{M}$. The purpose of smoothing the potential is not only to avoid the singularity at the position of the secondary, but to mimic the vertically integrated forces that the two-dimensional fluid elements feel within a scale height of the BH (see Tanaka et al. 2002; Masset 2002; Müller et al. 2012).

While the disc is initially steady, it experiences perturbations in response to the placement of the secondary BH. These perturbations are transient and decay after a viscous time. The viscous time is given by

$$t_{\rm visc}(r) = \frac{2}{3} \frac{r^2}{\nu} = \frac{M^2}{3\pi\alpha} t_{\rm orb}(r) \approx 1415 \left(\frac{M}{20}\right)^2 \left(\frac{\alpha}{0.03}\right)^{-1} t_{\rm orb}$$
 (3)

where $v = \alpha c_s h = \alpha h^2 \Omega$, is the kinematic viscosity, and we define $t_{\rm visc}$ as a function of orbital time $t_{\rm orb}$ at the secondary location r. We therefore disregard the dynamics during the first 1400 orbits of the simulation when measuring the torques, to avoid including numerical transients. (Note that the secondary only moves a distance of $\sim 0.1 r_0$ during this phase.)

For a binary being driven together by gravitational waves, the

quadrupole approximation (Peters 1964) for the evolution of the orbital separation is

$$\dot{r}_{\rm GW} = -\frac{64}{5} \frac{(GM)^3}{c^5} \frac{1}{1+q^{-1}} \frac{1}{1+q} \frac{1}{r^3},\tag{4}$$

where G is the gravitational constant, c is the speed of light, and $M = M_1 + M_2$ is the total binary mass. Integrating this expression, the secondary's position can be written as

$$r(t) = r_{\min} \left[1 - 4R(t - t_{\text{total}}) \right]^{1/4}, \tag{5}$$

where t is the elapsed time, t_{total} is the total simulation time, r_{min} is the final separation at $t = t_{\text{total}}$, and $R \equiv \dot{r}_{\text{GW}}/r$ is the inspiral rate defined at the final separation. In principle, we have the choice of specifying the initial and final position of the secondary in code units, as well as the physical scale for the total mass M (note that $q = 10^{-3}$ has already been fixed). In practice, we are numerically limited by the total number of orbits we can simulate ($\approx 10,000$ at our chosen resolution). Our choice for, say r_{\min} and the physical mass scale, is further constrained in order for the binary to be chirping (i.e. changing its separation noticeably during the simulation), and for the GW frequency to fall in the LISA band. We therefore chose parameters that are appropriate for a LISA IMRI: $M_1 = 10^6 M_{\odot}$, $q = 10^{-3}$, $r_{\text{min}} = 5r_{\text{S}}$ (where $r_{\text{S}} = 2GM_1/c^2$ is the Schwarzschild radius). Our choice of covering $\sim 10,000 \ \text{orbits}$ leads to an initial position of the secondary BH being $r_{\text{max}} = 11r_{\text{S}}$. Simulation parameters are defined in Table 1. Note that in code units, $r_{\min} = 1$ (i.e. twice the inner boundary), $r_{\max} = 2.2$.

The potential remains Newtonian, despite the fact that the final stages of the inspiral we simulate here are close to the innermost stable circular orbit (ISCO) of the central SMBH ($r_{\rm isco}=3r_{\rm S}$ for a non-spinning BH). In reality the disc dynamics would be altered by relativistic effects, but we chose to start with the simpler, scale-free case before investigating more realistic additional physics in future work.

In a similar vein, throughout the inspiral we measure the torques exerted on the BH, but the BH does not respond to these torques. While restricting the BH to adhere to an imposed orbit is artificial, it does not break angular momentum conservation between the migrator and the disc (just as imposing $\dot{r}=0$ to enforce a stationary orbit does not lead to a spurious torque (Murray & Dermott 2000)). Not implementing a 'live' BH allows us to observe gas asymmetry and makes a single calculation scalable to any value of Σ_0 . As we show below, the migration rate of the BH is strongly dominated by GW emission, and gas torques only impart a very small deviation.

3.3 Accretion Prescription

To model accretion onto the migrating secondary BH (M_2) , we implement a sink prescription similar to Farris et al. (2014) and Tang et al. (2017). Within a sink radius centered on the BH, the surface density of the gas is reduced on the local viscous timescale, assuming the gas surrounding the secondary settles into a mini-disk with parameters M=20 and $\alpha=0.03$. The sink radius is set to be the smoothing length of the gravitational potential ϵ , since we do not resolve the BH's event horizon. There are 15 cells across the accretion sink, which in physical units extends to 125 Schwarzschild radii (in radius) of the secondary BH.

The accretion timescale for the secondary BH is given by the viscous time of the mini-disk, $t_{\text{visc}}(\epsilon) = (2/3)(\epsilon^2/\nu)$. This is implemented with a new source term, which reduces the surface

density inside the sink at the rate

$$\frac{d\Sigma}{dt} = -\frac{\Sigma}{t_{\text{visc}}} \exp{-(r_2/r_{\text{sink}})^4}.$$
 (6)

The exponential factor acts to smooth the sink radius boundary, in order to reduce numerical artifacts that arise from discontinuous changes in the surface density.

We caution that by utilizing an alpha disk model, choosing a mach number $\mathcal{M}=20$ implies an accretion rate for the disc to be in a steady state. For certain choices of parameters this rate can exceed the Eddington rate, where $\dot{M}_{\rm Edd}=L_{\rm Edd}/(\epsilon_{\rm eff}c^2)$, where $L_{\rm Edd}=4\pi Gc\kappa_{\rm es}^{-1}M$ is the Eddington luminosity, $\kappa_{\rm es}$ is the electron scattering opacity, and $\epsilon_{\rm eff}$ is the radiative efficiency.

For the accretion rate we adopt onto the secondary with Eq 6, our choice of $\mathcal{M}=20$ and $\alpha=0.03$ implies a super-Eddington accretion rate of *cite fraction of \dot{M}/\dot{M}_{Edd} * for discs denser than $\Sigma_0>$?. This presents an inevitable inconsistency, given we do not include radiation in our simulations, yet we are unable to simulate a disc that is sufficiently thin to correspond to a sub-Eddington accretion rate. (Thinner, colder discs are numerically challenging to simulate given their low sound speed and correspondingly small time steps.) Radiation may certainly play a role in the gas properties around the secondary. Although, it is worth mentioning radiation-hydrodynamic simulations by Jiang et al. 2014 of super-Eddington accretion that find radiation preferentially escapes the disc in the vertical direction, having little impact on the surrounding gas and the accretion rate.

For simplicity, we neglect the impact of radiation in the present work. In reality the accretion efficiency onto the secondary BH is uncertain, and our fiducial choice is an estimate. Future work will explore the dependence of the gas dynamics and torques on the accretion efficiency.

4 SIMULATION RESULTS

Here we define the various components of the torque exerted on the inspiraling BH before directly comparing them in the simulation.

The dominant mechanism for angular momentum loss of the secondary BH is GW emission (§ 4.1), for which the torque is derived from the quadrupole formula:

$$T_{\rm GW} = -\frac{1}{2} M_2 r \dot{r}_{\rm GW} \Omega_2. \tag{7}$$

Note that we are assuming the center of mass is at the position of the primary, Ω_2 is the Keplerian orbital frequency of the secondary, and we quote the torques exerted on the secondary.

Gas can impart a torque on the secondary in two different ways – by gravitational interaction and by accretion. The gravitational torque $T_{\rm g}$ arises from the gravitational force exerted by the gas. We calculate this torque by summing up the ϕ -component of the gravitational force ${\bf g}_{\phi}$ crossed with the binary lever arm ${\bf r}$ over all the grid cells in the disc,

$$T_{g} = \sum |\mathbf{g}_{\phi} \times \mathbf{r}| \tag{8}$$

where $|\mathbf{r}|$ is the separation of the binary. We describe this torque in detail in § 4.1 and distinguish between positive and negative contributions from different regions of the disc.

Accretion onto the BH is another mechanism for angular momentum gain/loss. Assuming that the relative linear momentum of

the accreted gas is added to the BH, the accretion torque $T_{\rm acc}$ is calculated by summing the relative momenta contributed by the cells within the sink radius:

$$T_{\rm acc} = \sum_{\rm sink} \dot{m} |\mathbf{v}_{\rm rel} \times \mathbf{r}|,\tag{9}$$

where $\mathbf{v}_{\rm rel} = \mathbf{v_i} - \mathbf{v}_{\rm BH}$ is the velocity of the gas relative to the BH, and \dot{m} is the accretion rate inside the sink, i.e. the integral of equation (6). As discussed in § 4.2 below, we find this component of the torque to be relatively insignificant.

Analytical estimates for Type II migration torques often utilise the viscous torque as a reference, which follows directly from equation (3) and is given by

$$T_{\nu} = -3\pi r^2 \Omega_2 \nu \Sigma. \tag{10}$$

The magnitude of gas torques (equations 8, 9, and 10) all depend linearly on the normalisation of the surface density, a parameter we are free to choose. Estimates for Σ vary by several orders of magnitude depending on the chosen accretion disc model. In a steady-state Shakura-Sunyaev disc (Shakura & Sunyaev 1976), Σ is determined primarily by the assumed accretion rate \dot{M} and the viscosity parameter α . In the inner regions of accretion discs where radiation pressure becomes dominant, Σ is heavily dependent on whether viscosity scales with the gas pressure or with the total pressure (including radiation). For the system we consider here, the inspiraling BH is deep within the radiation-pressure dominated zone. Despite the limitation that our simulations include only gas pressure, we adopt two estimates for our normalization Σ_0 (at the secondary's final radius at $r_{\min} = 5r_{\text{S}}$) for the inner regions of thin, near-Eddington accretion discs that utilise each of these assumptions, representing low- and high-end estimates which bracket the range of expected densities.

We normalise our disc densities to represent AGN accreting at near-Eddington rates with a radiative efficiency $\epsilon_{\rm eff}=0.1$. The low estimate is obtained from the seminal model for a thin, viscous accretion disc by Shakura-Sunyaev (i.e. α -disc; Shakura & Sunyaev 1973), in which the viscosity is proportional to the total (gas + radiation) pressure. For this model, the surface density in the radiation-pressure dominated inner region is given by

$$\Sigma_{\alpha} = 88.39 \left(\frac{\alpha}{0.03}\right)^{-1} \left(\frac{\dot{M}}{0.1 \dot{M}_{\rm Edd}}\right)^{-1} \left(\frac{r}{5r_{\rm S}}\right)^{3/2} \text{ g cm}^{-2}$$
 (11)

where the fiducial choice for the accretion rate is 10% of the Eddington rate. In case the viscosity is proportional only to the gas pressure (i.e. for a so-called β -disc), the surface density at the same accretion rate is much higher. We estimate the surface density in this second model (see Haiman et al. 2009) as

$$\Sigma_{\beta} = 1.55 \times 10^{7} \left(\frac{\alpha}{0.03}\right)^{-4/5} \left(\frac{\dot{M}}{0.1 \dot{M}_{Edd}}\right)^{3/5} \times \left(\frac{M}{10^{6} M_{\odot}}\right)^{1/5} \left(\frac{r}{5 r_{S}}\right)^{-3/5} \text{ g cm}^{-2}. \quad (12)$$

4.1 Gas torques versus the GW torque

The gas torques measured in the simulation, along with the GW torques, are compared in Fig. 2. All torques are shown scaled by the viscous torque and as a function of the evolving binary separation. The first point we address is the strength of the gas torques relative to the GW torque. The gas torque we measure differs from the analytical estimates (based on the viscous torque T_V) in both magnitude

	Simulation Parameters		
Chosen Parameters		[cgs]	[code]
α	Viscosity parameter	0.03	0.03
M	Mach number	20	20
ϵ	Smoothing length	$125 r_{\rm S}({\rm M}_2) = 3.7 \times 10^{10} {\rm cm}$	0.025
$r_{ m sink}$	Sink radius	$125 r_{\rm S}({ m M}_2)$	0.025
M _{BH}	Mass of primary BH	$10^6\mathrm{M}_\odot$	$GM_{BH} = 1.0$
q	Mass ratio M ₂ /M ₁	10^{-3}	10^{-3}
n _{orbits}	Total # of simulated binary orbits	9,721	9,721
r _{min}	Final binary separation	$5 r_{\rm S}(\rm M_1) = 1.5 \times 10^{12} \rm cm$	1.0
Derived parameters			
r/r	GW inspiral rate at final separation	$-2.59 \times 10^{-7} \mathrm{s}^{-1}$	-4.04×10^{-5}
r _{max}	Initial binary separation	$11r_{\rm S}(\rm M_1) = 3.3 \times 10^{12} \rm cm$	2.2
t _{total}	Total simulation time	$2.16 \times 10^7 \text{ s} = 0.68 \text{ yr}$	$22,088.3 \times 2\pi$
	LISA-related Parameters		
f_{min}	Initial GW frequency of binary	0.626 mHz	
f_{max}	Final GW frequency of binary	2.042 mHz	
z	Redshift (for detectability estimate)	1	
τ	LISA mission lifetime	5 yrs	
L	LISA arm length	2.5 million km	
N	Number of laser links	6	

Table 1. Definition of parameters used throughout the paper, with their adopted values in both physical and simulation units.

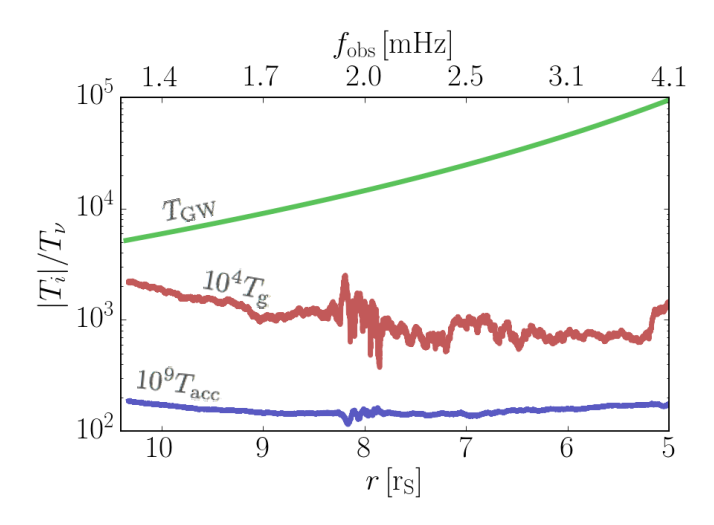


Figure 2. Different components of the total torque exerted on the secondary BH: gravitational torque (T_g) and accretion torque (T_{acc}) from the gas disc, as well as the torque from GW emission (T_{GW}) . All three torques are scaled by the fiducial viscous torque at the secondary's location. The gas torques are normalised to correspond to a β -disc (see equation 12). Note the overall different scale for each torque shown. The GW and accretion torques are both inward, while the gravitational torque is outward.

and direction. As Fig. 2 shows, the torque we find is 5 - 10 times weaker than T_v .

We compare the strength of the measured torque to analytical estimate following Syer & Clarke 1995, for which the secondary-dominated Type II torque is obtained by T_{ν} with a multiplicative factor given by the ratio of disc mass to satellite mass $(4\pi r^2 \Sigma_0/M_2)$ (Note this scaling of the torque is also found

in Duffell et al. 2014). We find that, assuming the α -disc mass, the simulated torque is ~ 8 orders of magnitude stronger than the analytical estimate. This is not surprising, given that the mass of the disc inside the secondary's orbit is relatively small when compared to the BH mass M_2 . If the estimate is provided by the denser β -disc, the simulated torque is still stronger by ~ 3 orders of magnitude.

Furthermore, for our disc parameters the gravitational torque causes the secondary the migrate *outward* rather than inward (outward torques in isothermal discs have also been noted by Duffell 2015a). The torque also changes with migration rate, decreasing in strength as the secondary BH moves inward and accelerates. For the case that the surface density is high, resulting in the strongest torque (in the β -disc model), the gas torque is still several orders of magnitude weaker than the GW torque (Fig. 3). Nevertheless migration can still produce a detectable deviation in the GW signal, as we discuss in § 5.

Our simulation results can be used to understand the origin of gas torques in more detail, and how the different components depend on the accretion or migration rate of the BH. The entirety of the disc exerts some gravitational force on the secondary BH, including both the inner and outer disc, streams across the gap, and gas near the BH itself. We include all of these regions to calculate the total gas torque.

We find that gas closest to the BH, particularly within the Hill sphere, is the dominant contributor to the torque due to its close proximity. The Hill sphere is an approximation of an embedded body's sphere of influence in the presence of a more massive body at a distance *a*. Its radius is estimated as

$$r_{\rm H} = \left(\frac{q}{3}\right)^{1/3} a. \tag{13}$$

As gas flows across the gap, it can continue to replenish the net angular momentum of material in the Hill sphere of the secondary. This can cause an asymmetry within the Hill sphere, and a slight increase in the gas density upstream from the BH, leading to a

consistently positive (outward) torque. This torque has been seen in other works (e.g. D'Angelo et al. 2005). Accurately capturing the gas morphology within the Hill sphere requires high spatial resolution. Further work investigating the gas streamlines, particularly with high-resolution 3-dimensional simulations, will likely be necessary to accurately measure the torque arising from this asymmetry, and to fully understand the reason for the small front-back asymmetry that yields the net torque.

We note that in disc-satellite calculations, the torque within the Hill sphere is often ignored or "damped", based on the assumption that material within the Hill sphere is bound to the perturber (e.g. de Val-Borro et al. 2006; Dürmann & Kley 2017). However, asymmetrically distributed gas in this region can exert a net torque on the BH, which must be included if the BH and the gas is separately resolved and followed. This asymmetry, unlike a bound 'orbiter', is constantly supplied as gas flows across the gap. In our case the accumulation of gas leading the BH's orbit occurs because gas preferentially flows ahead of the BH and/or because it slows down (and hence spends more time) in this region.

Further evidence for torque inside the Hill sphere is present in simulations by Crida et al. 2009, in which a live BH experiences changes in migration rate when torques within the Hill sphere are truncated. In their case the planet migrates inward more quickly when the Hill region is included, suggesting an accumulation of gas in the trailing side of the planet's orbit. This is likely due to a difference in disc parameters since the dynamics are sensitive to viscosity and mach number. Ultimately truncating the torque in the Hill sphere gives a poor approximation to a self-consistent, highly resolved torque calculation, which suggests that this region is important. Our simulations sufficiently resolve gas flow within the Hill sphere, and thus we choose to not omit this region when computing the total torque.

Fig. 3 shows the torque broken into two components – inside and outside the secondary's Hill sphere – along with smooth fits to the data which we use for calculating detectability in § 5. The Hill sphere torque is qualitatively different in that **it settles to a positive value (it pushes outward)**. The gas from elsewhere in the disc, including the inner and outer discs, as well as the streams connecting the two regions, exerts a negative (inward) torque that is 1-5% of the viscous torque. Fig. 4 shows 2D torque density contours of each of these components. The left panel illustrates the torque density outside of the Hill sphere, which is dominated by the streams flowing across the secondary BH's orbit. The right panel zooms in on the torque density inside the Hill sphere, showing that there is a slight density increase in the gas in front of the BH (for a counterclockwise orbit). This asymmetry is responsible for the positive torque.

4.2 Accretion torque

For the fiducial accretion rate, we find that the accretion torque is negligible compared to the gravitational torque from the gas – their magnitudes differ by ~ 6 orders of magnitude, as seen in Fig. 2. This is because the relative velocity of the gas near the black hole is effectively negligible. We show this in Fig. 5, with a snapshot of the velocity field in a frame co-rotating with the binary. The gas close to the BH has low angular momentum and resembles a quasi-stationary atmosphere, rather than a near-Keplerian mini-disc.

Accretion plays a minimal role in our simulations. The most conspicuous effect of accretion is to reduce the density of the gas near the BH, which leads to a decrease in the positive component of the torque. Without including a sink, our results

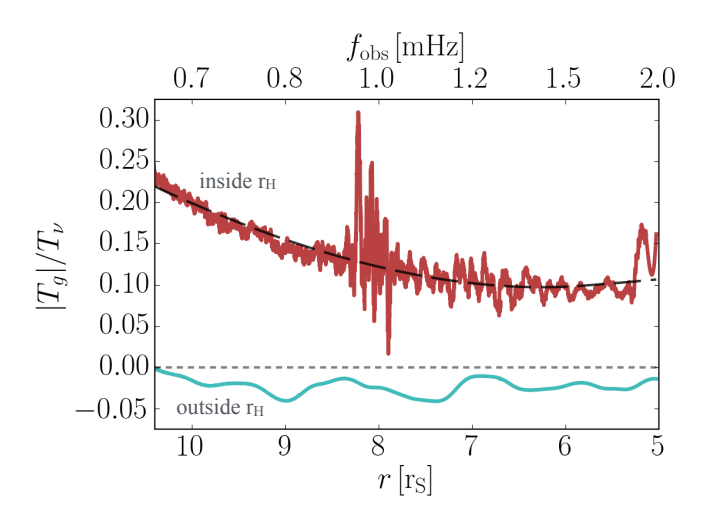


Figure 3. Gravitational torque T_g exerted by different regions of the gas disc onto the secondary BH, as a function of binary separation. The red (upper) curve shows torques from within the Hill sphere, and the green (lower) curve shows torques from outside this region. Both torques are scaled by the viscous torque. The dashed curve shows fitting formula we adopt for our LISA SNR computations (§ 5).

show the same asymmetry within the Hill sphere, albeit with more gas (and a larger positive component of the torque). The torque from elsewhere in the disk is unaffected by our sink prescription. We hypothesize that more efficient accretion would lead to more depleted gas density and less positive torque. This trend has been found in simulations of equal-mass binaries on fixed circular orbits, in which a sufficient increase in the accretion rate leads to a change in sign of the total torque (Tang et al. 2017). It is possible that a drastic increase in accretion rate could lead to other differences, since it would steal gas that would otherwise flow to the inner disc. We leave an investigation of the dependence of the torques on the accretion rate in the $q \neq 1$, GW-driven case to future work.

5 DETECTABILITY OF GAS IMPRINT BY LISA

5.1 Drift in the accumulated GW phase

In this section, we estimate the deviation from the vacuum GW signal caused by the gas disc torques, and assess its detectability by LISA.

The total accumulated phase of a gravitational wave event can be obtained by integrating over the total frequency evolution

$$\phi_{\text{tot}} = \int_{t_0}^{t_0 + t_{\text{obs}}} \dot{\phi}_{\text{GW}} \, dt = 2\pi \int_{t(f_{\text{min}})}^{t(f_{\text{max}})} f_{\text{GW}} \, dt$$
 (14)

where t_0 is an arbitrary reference time when the LISA observation begins, $t_{\rm obs}$ is the total observation time, $f_{\rm min}$ and $f_{\rm max}$ bracket the corresponding observed frequency range, $f_{\rm GW}(t) = \Omega(t)/\pi$ is the GW frequency, which is twice the binary's orbital frequency $\Omega(t)$, and $\phi_{\rm GW}$ is in radians. Assuming the orbit remains circular throughout the inspiral, changing the integration variable to orbital separation r gives

$$\phi_{\text{tot}} = -2\pi \int_{r_{\text{min}}}^{r_{\text{max}}} \frac{f_{\text{GW}}}{\dot{r}} \, d\mathbf{r}, \tag{15}$$

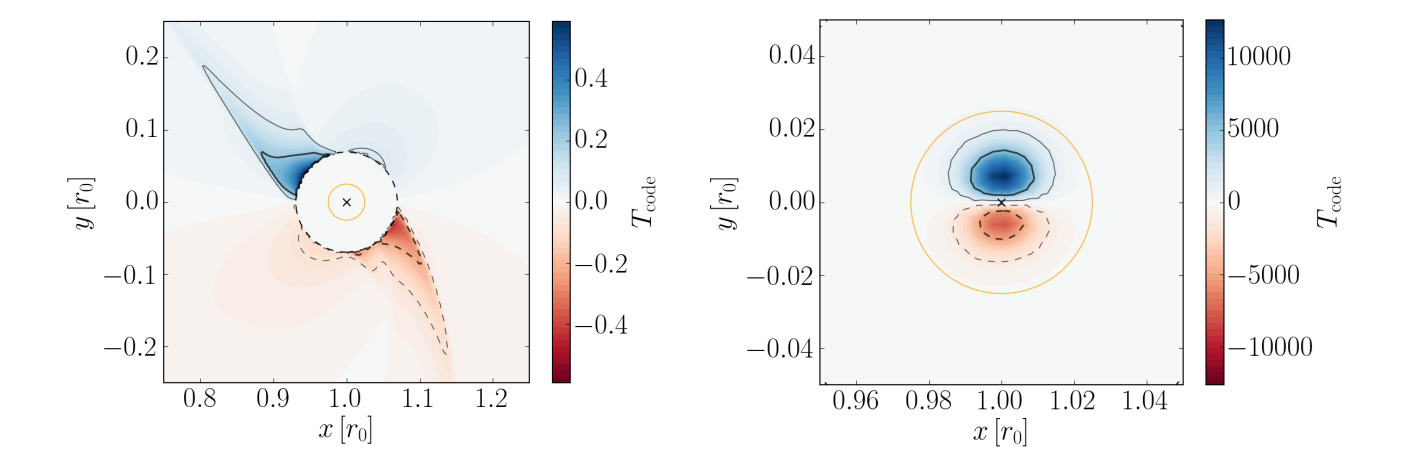


Figure 4. 2D contours of torque surface density, comparing the torques contributed by gas within the Hill sphere (right panel) to torques from gas outside this region (left panel).

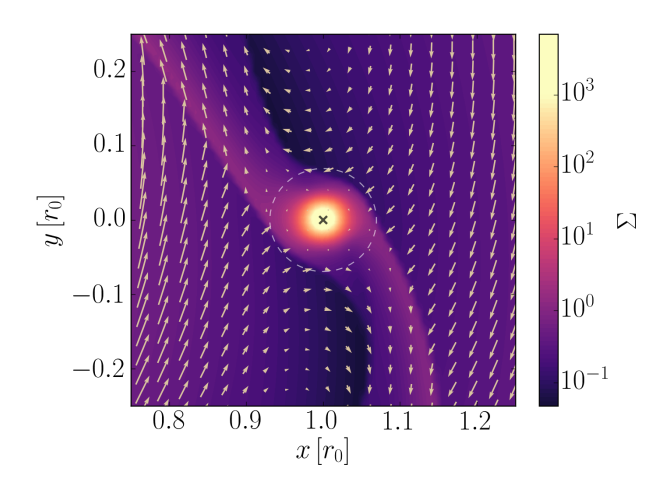


Figure 5. Velocity field in the frame co-rotating with the binary, overlaid on the surface density contour. Low relative velocities around the secondary BH indicate the build-up of a quasi-stationary atmosphere, rather than a near-Keplerian mini-disc.

where \dot{r} is the (negative) radial inspiral velocity corresponding to the angular momentum evolution of the binary. In our case, both GW emission and gas torques change the angular momentum, so the net evolution can be described by the sum of both components

$$\dot{r} = \dot{r}_{\rm GW} + \dot{r}_{\rm gas},\tag{16}$$

and the accumulated phase is given by

$$\phi_{\text{tot}} = -2\pi \int_{r_{\text{min}}}^{r_{\text{max}}} \frac{f_{\text{GW}}}{\dot{r}_{\text{GW}} + \dot{r}_{\text{gas}}} \, dr.$$
 (17)

Because the effect of gas is much smaller than GWs ($\dot{r}_{\rm gas} \ll \dot{r}_{\rm GW}$) the difference between the accumulated phase with and without gas, $\delta\phi \equiv \phi_{\rm GW+gas} - \phi_{\rm GW}$, can be simplified as follows:

$$\delta\phi = 2\pi \int_{r_{\text{min}}}^{r_{\text{max}}} \frac{f_{\text{GW}} \dot{r}_{\text{gas}}}{\dot{r}_{\text{GW}}^2} \left[1 + O\left(\frac{\dot{r}_{\text{gas}}}{\dot{r}_{\text{GW}}}\right)^2 \right] dr$$
 (18)

Our simulation provides a direct measurement of $\dot{r}_{gas}(\Sigma_0, r)$. We simplify the gravitational torque with a fit to the numerically measured value from the simulation. The fit for the total torque (adding the components inside and outside of the Hill sphere) has the form

$$T_{\rm fit} = \Sigma_0 (Ar^2 + Br + C) \tag{19}$$

with $A = 4.37 \times 10^{-28} \, \mathrm{cm^2 \, s^{-2}}$, $B = -8.16 \times 10^{-16} \, \mathrm{cm^3 \, s^{-2}}$, and $C = 4.19 \times 10^{48} \, \mathrm{cm^4 \, s^{-2}}$, This fitting formula is shown together with the numerically measured torques in Fig. 3. For $r < 6r_{\rm S}$, the spike at the end of the simulation is likely numerical, so in the range $3r_{\rm S} \le r \le 6r_{\rm S}$, we set the torque to remain a constant (we assume $3r_{\rm S}$ represents the end of the inspiral phase).

Using this fit for the total gas torque in equation (18) with the relation $\dot{r}_{\rm gas} = 2\dot{\ell}_{\rm gas} r^{1/2} (GM)^{-1/2}$ (where $\dot{\ell}_{\rm gas} = T_{\rm gas}/M_2$ is the rate of change of the secondary's specific angular momentum), we compute the phase drift $\delta\phi$ over an observed frequency window from $f_{\rm min}$ to $f_{\rm max}$. Unless stated otherwise, we use the total gas torque, including the contribution inside the Hill sphere.

5.2 Signal to noise ratio of the waveform deviation

To estimate the detectability of deviations from the vacuum inspiral waveform, we compute the signal—to—noise ratio (SNR) of the deviation produced by gas, compared to an event occurring in vacuum. The detectability of the gas-induced phase drift in an event depends on the strength of the torque (and thus linearly on the disc mass) as well as the frequency range of the LISA observation, since this determines the loudness of the event (the strain amplitude h), the number of observed orbits during which the phase drift can accumulate, and the instrumental noise.

The sky- and polarization-averaged GW strain amplitude of a source at comoving coordinate distance r(z) is

$$h = \frac{8\pi^{2/3}}{10^{1/2}} \frac{G^{5/3} \mathcal{M}_c^{5/3}}{c^4 r(z)} f_r^{2/3},\tag{20}$$

where $\mathcal{M}_c = M_1^{3/5} M_2^{3/5} / (M_1 + M_2)^{1/5}$ is the chirp mass and $f_r = f(1+z)$ is the rest-frame GW frequency (e.g. Sesana et al. 2005).

The *characteristic* strain h_c of a periodic source takes into

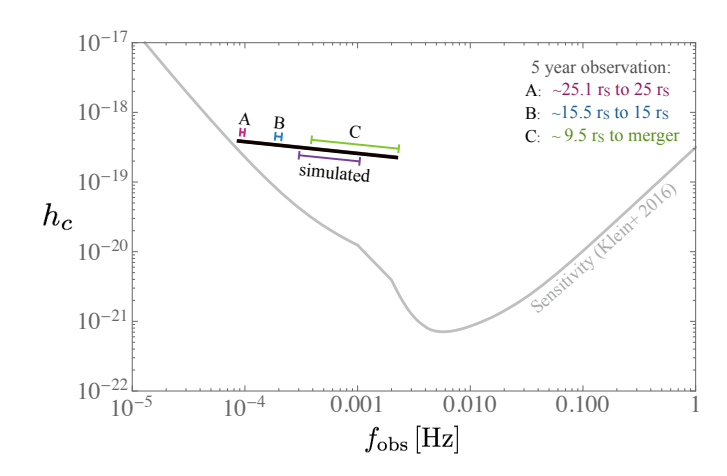


Figure 6. The characteristic strain amplitude of the binary inspiral, for an $M_1 = 10^6 M_{\odot}$, $M_2 = 10^3 M_{\odot}$ IMRI at redshift z = 1, as a function of the observed GW frequency. The top bracketed regions delineate three different 5-year observation windows as labeled, and the bottom bracket highlights the portion we cover in our simulation ($\sim 0.7 \text{yr}$).

account the total observation time τ (i.e. the LISA mission lifetime) as well as the characteristic number of cycles the source spends in each frequency band, $n = f^2/f$. For illustrative purposes, in Fig. 6 we plot the characteristic strain of an IMRI with our chosen mass ratio $q = 10^{-3}$, primary mass $M_1 = 10^6 M_{\odot}$ and redshift z = 1. The top bracketed regions highlight the evolution of the binary during three different possible 5-year long observational periods. The bottom bracketed portion delineates the evolutionary track we cover in our simulation, which corresponds to ~ 0.7 years. The torques outside this regime are extrapolated using the fitting formula (eq. 19).

Following Kocsis et al. (2011), the phase drift $\delta \phi$ can be expressed by the strain *deviation* $\delta \tilde{h}$ in Fourier space. If the Fourier amplitude strain of a vacuum waveform is \tilde{h} , the difference in strain due to the phase drift is given by

$$\delta \tilde{h} = \tilde{h}(1 - e^{i\delta\phi}),\tag{21}$$

assuming the gas-impacted and vacuum waveforms differ only in phase. The SNR of the deviation $\delta\rho$ can be computed in Fourier space as

$$(\delta \rho)^2 = 2 \times 4 \int_{f_{\min}}^{f_{\max}} df \frac{|\delta \tilde{h}(f)|^2}{S_n^2(f)f^2},\tag{22}$$

where $S_n(f)$ is the LISA sensitivity per frequency bin taken from Klein et al. (2016). The factor of 4 comes from the normalization of the one-sided spectral noise density, and the extra factor of 2 arises from the currently proposed configuration of LISA having 6 links, or effectively two interferometers. Similarly, the total SNR of the event is

$$\rho^{2} = 2 \times 4 \int_{f_{\min}}^{f_{\max}} df \frac{|\tilde{h}(f)|^{2}}{S_{n}^{2}(f)f^{2}},$$
(23)

The total inspiral for this particular binary takes ~ 100 years after the strain enters the LISA frequency band (at $f_{\rm min} \sim 10^{-4} {\rm Hz}$), so the total SNR depends on what separation the binary is at (or what GW frequency the binary is emitting) when the LISA observation

begins. The top panel in Fig. 7 shows the SNR of the gas-induced deviation as a function of the disc surface density Σ_0 and the phase drift $\delta\phi$ for three different 5–year observed frequency windows. Vertical lines in the figure mark the two estimates of the surface density for near-Eddington accretion discs (Eqs. 11 and 12). Initially the SNR scales linearly with surface density, before it saturates around a particular value once $\delta\phi\approx2\pi$.

The bottom panel of Fig. 7 shows the ratio of the SNR of the deviation compared to that of the total event, $\delta\rho/\rho$. By dividing out the total SNR, this quantity isolates the impact of the gas. For the case where the SNR of the deviation is highest (the green curve in Fig. 7), the SNR never reaches a saturated value because as the binary chirps towards merger, the change in the GW frequency results in a considerable contribution to $(\delta\rho)^2$ from a broad range of higher frequencies. While the influence of gas is comparatively stronger than GWs during the earlier stages of the inspiral, the detectability is less likely because a smaller frequency range results in a weaker SNR.

The SNR of the deviation (top panel in Fig. 7) is directly relevant to the detectability, and is dependent both on the strength of the deviations introduced by the gas, as well as on the total SNR of the event. While gas effects are stronger in the earlier stages of the inspiral, the overall SNR obtained by observing these stages (regardless of any phase change) is relatively low. If LISA catches the binary 5 years prior to merger, however, where its initial restframe separation is $r_{\min} \sim 10r_{\rm S}$, it will accumulate a significant amount of SNR as the binary chirps to merger, largely because the LISA noise is much lower towards higher frequencies (see Fig. 6). Thus for this particular binary, the deviation is most detectable in the final five years of the inspiral. This would not necessarily be the case, however, for lower-mass primary BHs, or lower-redshift events, which would chirp past the minimum of the noise curve. Adopting the criterion of detectability $\delta \rho \geq 10$, we find that the gas imprint is detectable for our fiducial binary if the BH is embedded in gas with surface density $\Sigma_0 \gtrsim 10^3 \, \mathrm{g \, cm^{-2}}$.

6 DISCUSSION AND CAVEATS

In the present work we find that, depending on the AGN disc mass, LISA can detect the migration imprint on gas-embedded IMRIs in the final 5 years of the inspiral. With our current understanding of AGN, the typical density of accretion discs is uncertain, and theoretical estimates range from $\Sigma \sim 10^1-10^8~{\rm g~cm^{-2}}$ in the regions of interest ($\lesssim 30r_{\rm S}$). We find that the deviation is detectable (SNR > 10) if the secondary BH is embedded in a disc with a surface density $\Sigma \gtrsim 10^3~{\rm gcm^{-2}}$. This density is reasonably reached in models of near-Eddington accretion discs; in particular it is exceeded in so-called β -discs. In our fiducial α -disc model, the torques are too weak to detect.

The difference between Σ in these models lies in the physical mechanism providing the viscosity and its dependence on radiation pressure, an area of active research in accretion disc dynamics (see Blaes et al. 2011; Jiang et al. 2013). The viscosity in β -discs, in particular, is assumed not to rise with radiation pressure. As a result, it is much lower than in the α -discs, resulting in a much higher disc surface density at a fixed accretion rate. If the signatures of a gas-embedded IMRI are detected by LISA, then it should be possible to extract information about the underlying disc, as even a measurement of a total accumulated phase shift will provide (at the least) a lower limit on the disc density. If both the amplitude and frequency-dependence of the deviation in the GW signal are

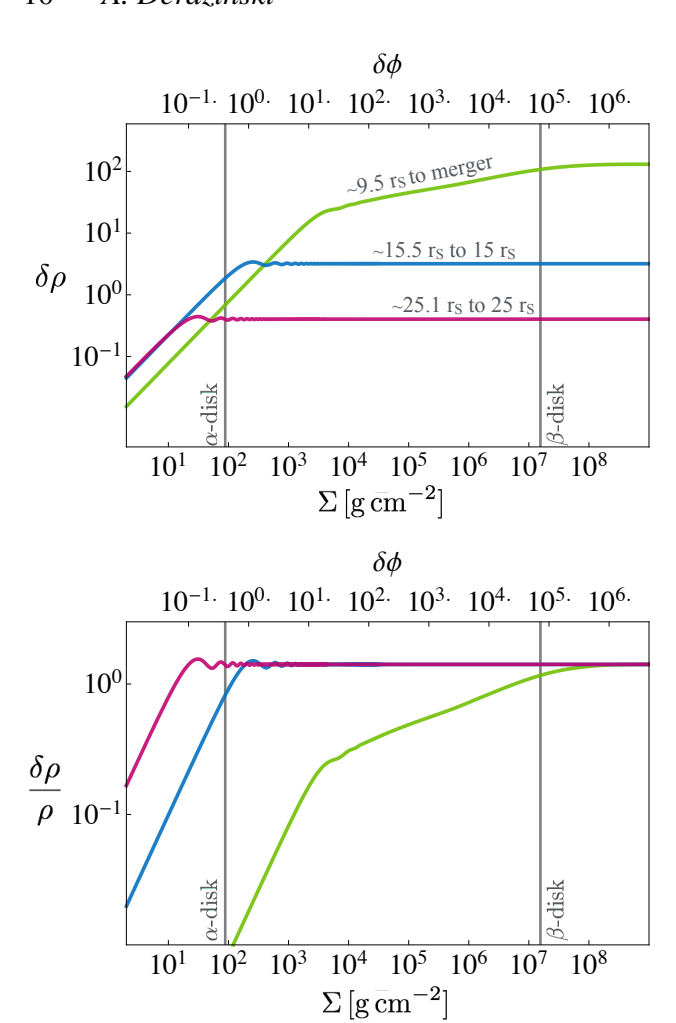


Figure 7. The top panel shows the SNR of the gas-induced deviation ($\delta\rho$; eq. 22) in the LISA waveform as a function of disc density, for different 5-year observation windows, and with our fiducial parameters $M=10^6 {\rm M}_\odot$, $q=10^{-3}$, and z=1. The lines are labeled with the binary's rest-frame separation during the LISA observation, with an assumed total observation time of 5 years. The top axis shows the corresponding total accumulated phase drift for each surface density, for the (ideal) case of observing the final 5 years to merger (green line). The lower panel shows the relative SNR: the SNR of the deviation in units of the total SNR of the event ($\delta\rho/\rho$; with ρ from eq. 23).

well measured, this will directly probe the density, and we expect other disc parameters to be constrained as well (e.g. density gradient, temperature, viscosity) provided the frequency-dependence amongst these parameters is well understood and not degenerate. Our basic conclusion is that LISA will have to opportunity to probe disc migration physics via gravitational waves.

We find that the effect of migration torques is stronger during the earlier stages of the inspiral, but its detectability is highest at higher frequencies, where LISA is most sensitive, and the system is chirping rapidly. For our fiducial binary ($M_1 = 10^6 M_{\odot}$, $q = 10^{-3}$, z = 1), the gas-induced deviation is most detectable during the final years of the inspiral, as this is when LISA accumulates most of the total SNR for the event. This feature is characteristic of the particular (redshifted) chirp mass, for which the last several cycles of the coalescence occur at frequencies near the minimum of the LISA sensitivity curve (see Fig. 6). For IMRIs with a higher chirp mass

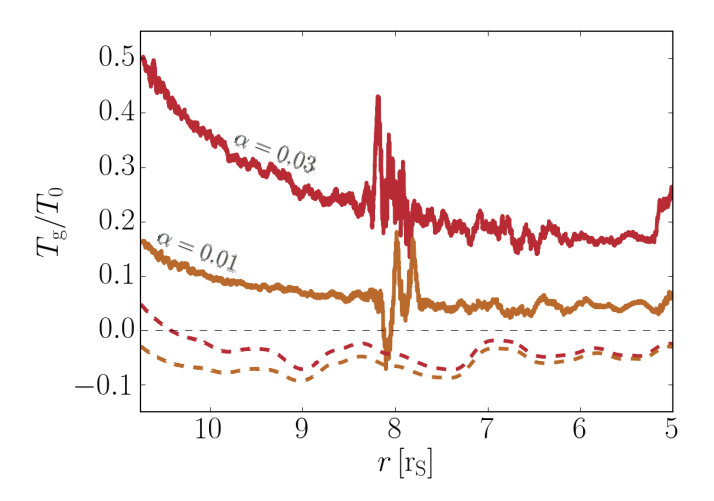


Figure 8. Torques exerted on the secondary BH from gas within the Hill sphere (solid curves) and outside the Hill sphere (dashed curves), for two runs with different viscosity parameter α as labeled. The torque from gas inside the Hill sphere is highly sensitive to the viscosity.

the merger will occur more quickly, the characteristic frequency is shifted to lower values, and we expect the contribution to the SNR from the final stages to be lower. The same may be true for lower chirp masses, which shift the final few cycles to higher frequencies past the minimum of the LISA noise curve. We plan to explore the range of detectability over various system parameters in future work.

It is worth noting that the torques depend on both disc physics and the accretion efficiency of the secondary BH. In particular, simulations of equal-mass binaries find that the build-up of gas within and near the Hill sphere, and therefore the net torque, scales with viscosity (Tang et al. 2017). To assess the sensitivity in our case, we re-run our fiducial calculation, except we reduced the viscosity by a factor of three. The evolution of the gas torques in both cases are compared in Fig. 8. We normalize the torques by the conventional Type I torque from Tanaka et al. (2002) provided by $T_0 = \sum r^2 \Omega^2 q^2 \mathcal{M}^2$, which does not depend on viscosity and thus allows for a direct comparison. As this figure shows, in the new run with $\alpha = 0.01$, the Hill sphere torque is 3 times weaker than in the $\alpha = 0.03$ case. On the other hand, the torques from outside the Hill sphere remain similar, and they tend to converge to the same value by the end of the inspiral. This suggests that the increase in the sink timescale (eq. 3) caused by the smaller α , is more important than the change in the dynamics due to the reduced viscosity in the bulk of the simulation, although we note that the reduced bulk viscosity may also play a role in reducing the gas flow around the secondary BH. We plan to further explore the sensitivity to α and to other parameters in future work.

We also note that in all cases, the migration torque exerted by the gas outside the Hill sphere is much weaker (by approximately an order of magnitude) than the torques from inside, and they also have the opposite sign (resulting in inward migration). Thus if the torques from inside the Hill sphere were excluded, the phase drift would be negative, corresponding to a slight increase in the inspiral rate, and the detectability would require an order of magnitude higher disc surface density.

Our detectability estimates are obtained for an intermediate mass ratio binary. For binaries with a more extreme mass-ratio, we expect that the gas effects would be more easily observable. First, a lower mass-ratio binary emits weaker GWs: the GW inspiral time is proportional to q^{-1} (at fixed total mass and binary separation measured in gravitational radii). The total number of cycles observed during the fixed LISA observation time scales with chirp mass as $\propto \mathcal{M}_c^{-5/8}$, yielding more cycles over which the phase drift can be measured for lower-mass companions. On the other hand, the scaling of the disc torques with mass ratio in the GW-driven regime is unknown and must be computed in future work. We note here only the following: If the gas-induced migration time-scale followed the viscous time, it would be independent of the secondary's mass M_2 . However, migration may be slower than the viscous timescale by a factor that depends on the ratio of the secondary and disc mass, $M_2/M_{\rm disc}$. In the self-similar models employed in Haiman et al. (2009), the migration timescale is proportional to $q^{-3/8}$, although Duffell et al. (2014) find a steeper, nearly linear scaling ($\propto q^{-1}$), approaching that of the GW torques. Finally, as the mass ratio decreases and the secondary BH no longer carves a gap, it will enter the Type I regime, in which the torque (provided by T_0) scales differently with mass ratio and disc parameters. As a comparison, if the secondary BH was instead a $10M_{\odot}$ BH (which for the disc parameters we adopt in this work, puts the BH in the Type I regime, see Duffell (2015b)) then the torque estimated by T_0 is ~ 3 orders of magnitude weaker than the torque exerted on our more massive, gapopening secondary. However, it is currently unclear how the torque changes with migration rate in this migration regime. Additionally, while IMRIs will characteristically have higher SNR, the current capabilities of numerical relativity are computationally limited for calculating waveforms for intermediate mass ratio systems (Mandel & Gair 2009). Accurate waveforms will be crucial for extracting the system parameters and for detecting a gas-induced phase drift.

An important question to consider is whether the impact of gas may be degenerate with system parameters (such as chirp mass, inclination, eccentricity, spin, etc.) or with other environmental effects, such as dynamical friction from dark matter (Barausse et al. 2015b). In principle, gas torques can also be degenerate with modifications to general relativity, although this effect would then be present in all E/IMRIs, while gas would have a variable effect from source to source. An exploration of the parameter space is beyond the scope of the present paper, and we leave it to future work. However, we note that the frequency dependence of the gas torque is generally different from that of the system parameters. At least for high SNR measurements for a source that chirps over a broad frequency band, and for which the frequency-dependence can be measured, we expect that the gas effects can be disentangled from system parameter variations (see discussion in Yunes et al. 2011).

We focus primarily on migration torques, but accretion discs can produce other interesting effects on BH inspirals that we neglect in the present study, including mass, spin, and eccentricity evolution. Efficient accretion can lead to a non-negligible increase in mass of the secondary BH throughout the inspiral, which will affect the GW frequency evolution (accretion onto the primary SMBH is negligible, as the increase in mass throughout the LISA lifetime is under the accuracy limit). The possibility exists for accretion to drive up the spins of the BHs (e.g. Teyssandier & Ogilvie 2017), an effect which we neglect here, and it may also act to align the spins of both BHs, particularly if the BHs form in the accretion disc (Bogdanović et al. 2007). While we do not model the spin of the BHs in this paper, we hypothesise that significant spin-up of the secondary is unlikely (at least for the prograde case we simulated here), because the relative angular momentum of the gas near the BH is low. This is shown in the velocity map in Fig. 5, where the gas around the BH exhibits properties more akin to an atmosphere than to a mini-disc.

Gas also provides the possibility for EM counterparts to the GW detection. If an associated EM signature is detected, it would confirm the presence of gas around the source. In this case, even a non-detection of a GW phase deviation for an EM-identified IMRI would teach us about the environment by putting a limit on the density and/or viscosity of the disc.

Simulations of intermediate-mass planets show that a disc may drive periodic eccentricity oscillations in the planet's orbit that are low but not negligible, with the eccentricity ranging from 0.01 to 0.1 (Ragusa et al. 2018, see also Papaloizou et al. 2001; Bitsch et al. 2013) although this depends on both the disc mass and the perturber mass (Dunhill et al. 2013). We expect that gas-embedded E/IMRIs will be close to circular compared to events originating from stellar remnants in galactic nuclei, which will have significantly higher eccentricities. Thus spin-aligned and near-circular events will be indicative of a gas disc.

In future work, we intend to relax several assumptions made in this study, as well as explore a range of values for the key parameters. In this paper we assumed a locally isothermal equation of state. This assumption should be relaxed by incorporating a more sophisticated treatment of the thermodynamics, allowing the gas to heat due to local shocks and viscous dissipation, and to cool through its surface (e.g. Farris et al. 2015a). It is also known that the α -prescription is a poor approximation in parts of the disc where the flow is not laminar, an issue that can be addressed using magneto-hydrodynamics simulations (e.g. Shi et al. 2012). As already mentioned above, a near-Eddington circumbinary accretion disc around a BH in the LISA band is likely to be supported by radiation pressure, which will need to be included in future simulations. Finally, our simulations in this study are in 2D. We expect that the 3D vertical structure will modify the structure of the gap and the accretion streams, as well as the gas distribution near the secondary BH, and will inevitably have a strong affect on the gas torques.

We also expect that the migration torques depend on disc parameters (such as α and \mathcal{M}), the density and temperature profiles of the disc, the BH mass ratio, any orbital eccentricity, and also the GW-driven orbital decay rate. Indeed, even for non-migrating planets, Duffell (2015a) find that disc torques are sensitive to combinations of these parameters, particularly in the intermediate mass-ratio regime.

Despite its limitations, our present study suggests that the impact of circumbinary gas may be measurable in the LISA waveform of an E/IMRI event and warrants further investigation. We intend to address the outstanding issues in future work.

7 CONCLUSIONS

In this paper, we study the gas torques exerted on a gravitational wave driven inspiral with high resolution 2D hydrodynamic simulations of a 10^{-3} mass ratio binary in an isothermal viscous disc. Motivated by the prospect of LISA detecting the late stages of intermediate mass ratio inspirals, we apply the results of our simulations to estimate the detectability of gas torques on a $10^6 M_\odot + 10^3 M_\odot$ binary merger occurring at a redshift z=1.

We find that the net disc torque differs from previous semi-analytic estimates, which were based on the viscous torque for a non-migrating secondary. While these previous torque estimates were negative, we here find that the total torque is positive, resulting in a slow-down of the inspiral, and its strength is only fraction (1%-5%)

of the viscous torque. While it is 4-5 orders of magnitude weaker than the torque due to GW emission, it can still produce a detectable phase drift in the GW waveform. For our fiducial estimate of the accretion rate, the accretion torque is at least 10-11 orders of magnitude weaker than that due to GWs and does not contribute significantly to the gas imprint in the waveform.

An analysis of the origin of the torques shows that gas very close to the secondary BH (inside its Hill sphere) exhibits a front-to-back asymmetry with respective to the direction of the secondary's motion, and leads to the positive (outward) component of the torque, whereas gas elsewhere in the disc exerts a weaker negative torque. More sophisticated simulations that resolve the 3-dimensional gas morphology **and velocity of gas** near the secondary BH could provide insight into whether and how this asymmetry occurs.

For the IMRI we consider here, the deviation in the GW waveform is detectable (with a signal to noise ratio >10) if the system is embedded in a disc with a surface density $\Sigma_0\gtrsim 10^3~{\rm gcm}^{-2}$. This density may be exceeded in cold, thin, near-Eddington discs expected in active galactic nuclei. Gas-induced deviations are strongest during the earlier stages of the inspiral, but they are more detectable for binaries at higher frequencies, where LISA's sensitivity is stronger and the binary is chirping significantly. We expect the gas disc-induced phase drift in the GW waveform to be sensitive to disc properties, which implies that the detection of a gas-embedded inspiral will provide the opportunity for LISA to probe the physics of AGN discs and migration torques.

AMD acknowledges support by the National Science Foundation (NSF) Graduate Research Fellowship under Grant DGE 1644869. The authors acknowledge financial support from NSF grants DGE 1715661 and AST-1715356, NASA grants NNX17AL82G, 16-SWIFT16-0015, and Einstein Postdoctoral Fellowship award number PF6-170151 (DJD).

REFERENCES

```
Amaro-Seoane P., Gair J. R., Freitag M., Miller M. C., Mandel I., Cutler
   C. J., Babak S., 2007, Classical and Quantum Gravity, 24, R113
Amaro-Seoane P., et al., 2017, preprint, (arXiv:1702.00786)
Barausse E., Cardoso V., Pani P., 2014, Phys. Rev. D, 89, 104059
Barausse E., Bellovary J., Berti E., Holley-Bockelmann K., Farris B.,
    Sathyaprakash B., Sesana A., 2015a, in Journal of Physics Con-
    ference Series. p. 012001 (arXiv:1410.2907), doi:10.1088/1742-
    6596/610/1/012001
Barausse E., Cardoso V., Pani P., 2015b, in Journal of Physics Con-
    ference Series. p. 012044 (arXiv:1404.7140), doi:10.1088/1742-
   6596/610/1/012044
Barnes J. E., Hernquist L., 1996, ApJ, 471, 115
Bartos I., Kocsis B., Haiman Z., Márka S., 2017, ApJ, 835, 165
Baruteau C., Ramirez-Ruiz E., Masset F., 2012, MNRAS, 423, L65
Baruteau C., et al., 2014, Protostars and Planets VI, pp 667-689
Bellovary J. M., Mac Low M.-M., McKernan B., Ford K. E. S., 2016, ApJ,
Bitsch B., Crida A., Libert A.-S., Lega E., 2013, A&A, 555, A124
Blaes O., Krolik J. H., Hirose S., Shabaltas N., 2011, ApJ, 733, 110
Bogdanović T., Reynolds C. S., Miller M. C., 2007, ApJ, 661, L147
Cerioli A., Lodato G., Price D. J., 2016, MNRAS, 457, 939
Chakrabarti S. K., 1996, Phys. Rev. D, 53, 2901
Chang P., Strubbe L. E., Menou K., Quataert E., 2010, MNRAS, 407, 2007
Crida A., Morbidelli A., 2007, MNRAS, 377, 1324
Crida A., Baruteau C., Kley W., Masset F., 2009, A&A, 502, 679
D'Angelo G., Bate M. R., Lubow S. H., 2005, MNRAS, 358, 316
D'Orazio D. J., Loeb A., 2018, Phys. Rev. D, 97, 083008
Dotti M., Sesana A., Decarli R., 2012, Advances in Astronomy, 2012,
    940568
```

```
Duffell P. C., 2016, ApJS, 226, 2
Duffell P. C., Haiman Z., MacFadyen A. I., D'Orazio D. J., Farris B. D.,
    2014, ApJ, 792, L10
Dunhill A. C., Alexander R. D., Armitage P. J., 2013, MNRAS, 428, 3072
Dürmann C., Kley W., 2017, A&A, 598, A80
Edgar R. G., 2007, ApJ, 663, 1325
Farris B. D., Duffell P., MacFadyen A. I., Haiman Z., 2014, ApJ, 783, 134
Farris B. D., Duffell P., MacFadyen A. I., Haiman Z., 2015a, MNRAS, 446,
Farris B. D., Duffell P., MacFadyen A. I., Haiman Z., 2015b, MNRAS, 447,
    L80
Fontecilla C., Chen X., Cuadra J., 2017, MNRAS, 468, L50
Goldreich P., Tremaine S., 1980, ApJ, 241, 425
Goodman J., Tan J. C., 2004, ApJ, 608, 108
Goulding A. D., et al., 2018, PASJ, 70, S37
Haiman Z., Kocsis B., Menou K., 2009, ApJ, 700, 1952
Hopkins P. F., Hernquist L., Cox T. J., Kereš D., 2008, ApJS, 175, 356
Ivanov P. B., Papaloizou J. C. B., Polnarev A. G., 1999, MNRAS, 307, 79
Janiuk A., Bejger M., Charzyński S., Sukova P., 2017, New Astron., 51, 7
Jiang Y.-F., Stone J. M., Davis S. W., 2013, ApJ, 778, 65
Jiang Y.-F., Stone J. M., Davis S. W., 2014, ApJ, 796, 106
Kauffmann G., Haehnelt M., 2000, MNRAS, 311, 576
Kennedy G. F., Meiron Y., Shukirgaliyev B., Panamarev T., Berczik P., Just
    A., Spurzem R., 2016, MNRAS, 460, 240
Klein A., et al., 2016, Phys. Rev. D, 93, 024003
Kocsis B., Sesana A., 2011, MNRAS, 411, 1467
Kocsis B., Yunes N., Loeb A., 2011, Phys. Rev. D, 84, 024032
Levin Y., 2007, MNRAS, 374, 515
Mandel I., Gair J. R., 2009, Classical and Quantum Gravity, 26, 094036
Masset F. S., 2002, A&A, 387, 605
Mayer L., 2013, Classical and Quantum Gravity, 30, 244008
McKernan B., Ford K. E. S., Lyra W., Perets H. B., 2012, MNRAS, 425,
McKernan B., Ford K. E. S., Kocsis B., Lyra W., Winter L. M., 2014,
    MNRAS, 441, 900
McKernan B., et al., 2017, preprint, (arXiv:1702.07818)
Miller M. C., 2009, Classical and Quantum Gravity, 26, 094031
Müller T. W. A., Kley W., Meru F., 2012, A&A, 541, A123
Murray C. D., Dermott S. F., 2000, Solar System Dynamics
Narayan R., 2000, ApJ, 536, 663
Paardekooper S.-J., Mellema G., 2006, A&A, 459, L17
Papaloizou J. C. B., Nelson R. P., Masset F., 2001, A&A, 366, 263
Perna R., Lazzati D., Giacomazzo B., 2016, ApJ, 821, L18
Peters P. C., 1964, Phys. Rev., 136, B1224
Ragusa E., Rosotti G., Teyssandier J., Booth R., Clarke C. J., Lodato G.,
    2018, MNRAS, 474, 4460
Robert C. M. T., Crida A., Lega E., Méheut H., Morbidelli A., 2018, preprint,
    (arXiv:1808.00381)
Sesana A., Haardt F., Madau P., Volonteri M., 2005, ApJ, 623, 23
Sesana A., Roedig C., Reynolds M. T., Dotti M., 2012, MNRAS, 420, 860
Shakura N. I., Sunyaev R. A., 1973, A&A, 24, 337
Shakura N. I., Sunyaev R. A., 1976, MNRAS, 175, 613
Shi J.-M., Krolik J. H., Lubow S. H., Hawley J. F., 2012, ApJ, 749, 118
Stone N. C., Metzger B. D., Haiman Z., 2017, MNRAS, 464, 946
Syer D., Clarke C. J., 1995, MNRAS, 277, 758
Tanaka H., Takeuchi T., Ward W. R., 2002, ApJ, 565, 1257
Tanaka T., Menou K., Haiman Z., 2012, MNRAS, 420, 705
Tang Y., MacFadyen A., Haiman Z., 2017, MNRAS, 469, 4258
Tang Y., Haiman Z., MacFadyen A., 2018, MNRAS, 476, 2249
Tazzari M., Lodato G., 2015, MNRAS, 449, 1118
Teyssandier J., Ogilvie G. I., 2017, MNRAS, 467, 4577
Ward W. R., 1997, Icarus, 126, 261
Yi S.-X., Cheng K. S., Taam R. E., 2018, The Astrophysical Journal Letters,
    859, L25
Yunes N., Kocsis B., Loeb A., Haiman Z., 2011, Physical Review Letters,
    107, 171103
```

Duffell P. C., 2015a, ApJ, 806, 182

Duffell P. C., 2015b, ApJ, 807, L11

de Val-Borro M., et al., 2006, MNRAS, 370, 529